

Organic Fluorophore Coated Polycrystalline Ceramic LSO:Ce Scintillators for X-ray Bioimaging

Mary K. Burdette,^{†,‡} Yuriy P. Bandera,^{†,‡} Eric Zhang,^{†,‡} Artem Trofimov,[†] Ashley Dickey,[§] Isabell Foulger,^{||} Joseph W. Kolis,[§] Kelli E. Cannon,[‡] Aundrea F. Bartley,[#] Lynn E. Dobrunz,[#] Mark S. Bolding,[▽] Lori McMahon,[○] and Stephen H. Foulger^{*‡,||,◆,○}

[†]Department of Materials Science and Engineering, Clemson University, Clemson, South Carolina 29634, United States

[‡]Center for Optical Materials Science and Engineering Technologies, Clemson University, Anderson, South Carolina 29625, United States

[§]Department of Chemistry, Clemson University, Clemson, South Carolina 29634, United States

^{||}Department of Bioengineering, Clemson University, Clemson, South Carolina 29634, United States

[▽]Department of Vision Science, University of Alabama at Birmingham, Birmingham, Alabama 35294, United States

[#]Department of Neurobiology, Evelyn F. McKnight Brain Institute & Civitan International Research Center, University of Alabama at Birmingham, Birmingham, Alabama 35294, United States

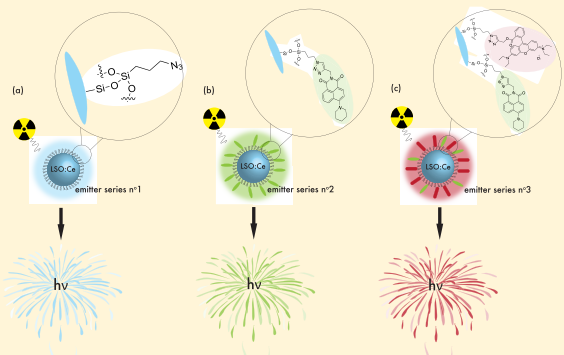
[◆]Department of Radiology, University of Alabama at Birmingham, Birmingham, Alabama 35294, United States

[○]Department of Cell, Developmental, and Integrative Biology, University of Alabama at Birmingham, Birmingham, Alabama 35294, United States

^{*}Department of Materials Science and Engineering, Clemson University, Clemson, South Carolina 29634, United States

Supporting Information

ABSTRACT: The current effort demonstrates that lutetium oxyorthosilicate doped with 1–10% cerium ($\text{Lu}_2\text{SiO}_5:\text{Ce}$, LSO:Ce) radioluminescent particles can be coated with a single dye or multiple dyes and generate an effective energy transfer between the core and dye(s) when excited via X-rays. LSO:Ce particles were surface modified with an alkyne modified naphthalimide (6-piperidin-1-yl-2-prop-2-yn-1-yl-1H-benzo[*de*]isoquinoline-1,3-(2*H*)-dione, AlNap) and alkyne modified rhodamine B (*N*-(6-diethylamino)-9-{2-[{(prop-2-yn-1-yloxy)carbonyl}phenyl]-3*H*-xanthen-3-ylidene}-*N*-ethylethananilinium, AlRhod) derivatives to tune the X-ray excited optical luminescence from blue to green to red using Förster Resonance Energy Transfer (FRET). As X-rays penetrate tissue much more effectively than UV/visible light, the fluorophore modified phosphors may have applications as bioimaging agents. To that end, the phosphors were incubated with rat cortical neurons and imaged after 24 h. The LSO:Ce surface modified with AlNap was able to be successfully imaged *in vitro* with a low-output X-ray tube. To use the LSO:Ce fluorophore modified particles as imaging agents, they must not induce cytotoxicity. Neither LSO:Ce nor LSO:Ce modified with AlNap showed any cytotoxicity toward normal human dermal fibroblast cells or mouse cortical neurons, respectively.



INTRODUCTION

X-ray radiation is able to penetrate deeper into tissues than ultraviolet/visible light, which makes the use of X-rays for bioimaging and theranostic applications attractive.¹ Traditional uses of X-ray stimulation in bioimaging include X-ray projection imaging and computed tomography.^{2,3} More recently X-ray radiation has been utilized in advanced X-ray fluorescence computed tomography (XRCT),⁴ which utilizes positive contrast imaging agents to produce elemental maps of the tissue, and X-ray luminescence computed tomography (XLCT) that relies on the X-ray excitation and subsequent

optical detection of the imaging agent.^{5–8} These imaging agents employ molecules containing high atomic number elements due to their ability to absorb X-rays and downconvert the energy (i.e., scintillators). Once the scintillator is irradiated with high energy photons (such as those that come from X-ray or γ -ray radiation), electrons are promoted from the valence band to the conduction band, which leave behind holes in the

Received: September 18, 2018

Revised: December 4, 2018

Published: December 5, 2018



valence band. Either the electron–hole pairs travel through the conduction band until they reach the luminescent center or they get trapped in the conduction band by defects in the material. Trapped electron–hole pairs are omitted from the scintillation process and do not generate any light. The electron–hole pairs that reach the luminescent centers recombine and transfer their energy to the active center, which then emits visible light.^{9–13} For example, successful nanoparticle X-ray imaging agents include gadolinium containing compounds, such as gadolinium oxide,¹⁴ gadolinium oxysulfide doped with europium or terbium,¹⁵ sodium gadolinium tungstate,¹⁶ and alkali metal gadolinium fluorides doped with europium.⁷ Additional imaging agents that have been recently utilized for X-ray radiation induced bioimaging include lanthanum oxysulfide doped with europium or terbium¹⁵ and alkali metal yttrium fluorides doped with both ytterbium and erbium¹⁷ or gadolinium.¹⁸

While changing the phosphor to suit various emission needs is an option, many scintillators are hygroscopic, meaning that they lose their scintillation properties upon being in a water-rich environment.^{19–21} Therefore, these compounds are not suitable for use as bioimaging agents. While recent investigations into color-tuning of perovskite nanocrystals based on counterion type and concentration have shown promise, these materials may induce toxicity as there is no shielding of these particles from their environment.²² It would be desirable to use a bright, non-hygroscopic scintillating particle whose emission can be tuned by attaching an organic fluorophore, or multiple fluorophores, with various emission characteristics; however, these materials systems have not been studied in depth.^{23–25} To this end, we demonstrate that a lutetium oxyorthosilicate doped with cerium ($\text{Lu}_2\text{SiO}_5\text{:Ce}$, LSO:Ce) particle can be coated with a single fluorophore or multiple fluorophores and generate an effective energy transfer between the dye and core when excited through X-ray radiation. Furthermore, we show that the fluorophore coated LSO:Ce particles could be directly imaged with X-rays after incubation with rat cortical neurons. The particles as bare LSO:Ce or single fluorophore coated LSO:Ce were shown to be non-cytotoxic to normal human dermal fibroblast cells and rat cortical neurons, respectively. These fluorophore coated LSO:Ce particulates are promising candidates for applications as X-ray excited optical luminescence imaging agents.

EXPERIMENTAL SECTION

Reagents and Solvents. All reagents were purchased from commercial suppliers, such as Aldrich or Alfa Aesar, and were used without purification. All solvents used for reactions were distilled under nitrogen after drying over an appropriate drying reagent. LSO:Ce phosphors (median particle size: 4 μm) were purchased from Phosphor Technologies. To decrease the size of the phosphor particles, the particles were ball milled, and a final size of ca. 800 nm as measured by a Coulter N4 Plus DLS (dynamic light scattering) instrument was obtained. Deionized water was obtained from a Nanopure system and exhibited a resistivity of 18.2 M $\Omega\text{-cm}$. Analytical thin-layer chromatography was performed on glass plates coated with 0.25 mm 230–400 mesh silica gel containing a fluorescent indicator. Column chromatography was performed using silica gel (spherical neutral, particle size 63–210 μm).

Chemical Characterization Methods. ^1H NMR spectra were recorded on a JEOL ECX300 spectrometer. Chemical shifts for protons are reported in parts per million downfield from tetramethylsilane and are referenced to residual protium in the NMR solvent (CDCl_3 ; δ 7.26 ppm).

Syntheses. *6-(Piperidin-1-yl)-2-(prop-2-yn-1-yl)-1H-benzo[de]isoquinoline-1,3(2H)-dione (AlNap).* The 6-(piperidin-1-yl)-2-(prop-2-yn-1-yl)-1H-benzo[de]isoquinoline-1,3(2H)-dione was syn-

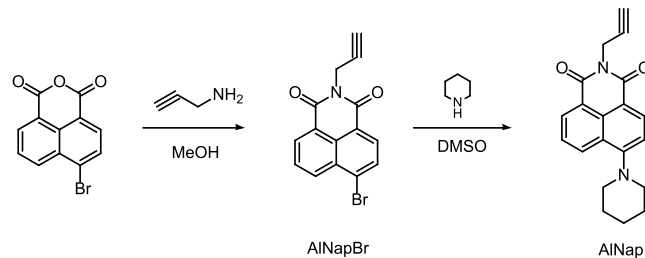


Figure 1. Synthesis of 6-(piperidin-1-yl)-2-(prop-2-yn-1-yl)-1H-benzo[de]isoquinoline-1,3(2H)-dione (AlNap).

thesized according to a previously reported method²⁶ (cf. Figure 1). ^1H NMR (CDCl_3): δ 1.73 (m, 2H), 1.89 (m, 4H, J = 5.5 Hz), 2.17 (t, 1H, J = 2.4 Hz), 3.24 (t, 4H, J = 5.5 Hz), 4.95 (d, 2H, J = 2.4 Hz), 7.18 (d, 1H, J = 8.3 Hz), 7.68 (d,d, 1H, J = 7.2 Hz), 8.40 (d,d, 1H, J = 8.3 Hz, J = 1.4 Hz), 8.53 (d, 1H, J = 8.3 Hz), 8.61 (d,d, 1H, J = 7.2 Hz, J = 1.4 Hz).

Mono(N-(6-(diethylamino)-1-(2-((prop-2-yn-1-yloxy)carbonyl)phenyl)-3H-xanthen-3-ylidene)-N-ethylethanaminium) Monocarbonate (AlRhod). Mono(N-(6-(diethylamino)-1-(2-((prop-2-yn-1-yloxy)carbonyl)phenyl)-3H-xanthen-3-ylidene)-N-ethylethanaminium) monocarbonate (AlRhod) was synthesized according to a previously reported method²⁷ (cf. Figure 2). ^1H NMR (CDCl_3): δ 1.33 (t, 12H, J = 7.2 Hz), 2.42 (t, 1H, J = 2.4 Hz), 3.65 (m, 8H, J = 7.2 Hz), 4.62 (d, 2H, J = 2.4 Hz), 6.84 (d, 2H, J = 2.4 Hz), 6.92 (m, 2H, J = 9.3 Hz, J = 2.4 Hz), 7.05 (d, 2H, J = 9.3 Hz), 7.34 (d, 1H, J = 7.6 Hz), 7.75 (m, 1H, J = 7.6 Hz), 7.85 (m, 1H, J = 7.6 Hz), 8.31 (d, 1H, J = 7.6 Hz).

(3-Azidopropyl)trimethoxysilane (1). The (3-chloropropyl)trimethoxysilane (1 g, 5.03 mmol) and sodium azide (0.684 g, 10.1 mmol) were mixed with dry dimethylformamide (3 mL), and the obtained mixture was stirred at 90 °C for 1 h. After cooling, the mixture was diluted with dry dichloromethane (10 mL) and filtered. The filtrate was collected and evaporated under vacuum to give a 25% solution of product in DMF. This solution was used in the next step. ^1H NMR (CDCl_3): δ 0.68 (t, 2H, J = 8.3 Hz), 1.70 (m, 2H, J = 6.9 Hz, J = 8.3 Hz), 3.25 (t, 2H, J = 6.9 Hz), 3.56 (s, 9H).

Synthesis of Emitter Series 1. LSO:Ce particles (average size 800 nm) (2 g) were mixed with methanol (15 mL), and the obtained suspension was sonicated for 15 min. Then the solution of 1 in DMF (1.4 mL) was added, and the mixture was stirred for 1 min. Finally, the aqueous solution of ammonium hydroxide (29%, 1 mL) was added to the mixture and stirred for 24 h; then the reaction was refluxed for 2 h. After cooling, the particles were separated by centrifugation, washed with methanol three times, and dried under vacuum at room temperature. The product afforded was azide modified LSO:Ce particles (cf. Figure 3a). Yield 2 g.

Synthesis of Emitter Series 2. The synthesis of emitter series 2 was performed by utilizing a standard copper catalyzed azide–alkyne cycloaddition (CuAAC) reaction. Emitter series 1 (300 mg) was dispersed in THF (2 mL) and added to the reaction vessel. Then AlNap (40 mg, 0.126 mmol) in THF (1 mL) was added to the reaction mixture. Finally, copper(II) sulfate (62.7 mg, 0.251 mmol) in deionized water (DI-water; 1 mL) and sodium ascorbate (124.5 mg, 0.628 mmol) in DI-water (1 mL) were added to the reaction vessel. Then the reaction vessel was placed in the J-KEM mini-reactor with stirring at 28 °C in the dark with a nitrogen purge. The reaction was allowed to proceed for 24 h. Upon reaction completion, the product was washed with THF. Then the product was washed with a water/EDTA solution to remove the copper catalyst. Finally, the product was washed six more times with THF. Washes were performed to remove any unattached dye from the particles. All washes were

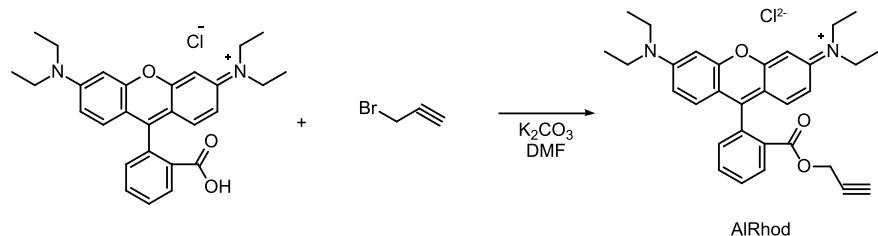


Figure 2. Synthesis of mono(N-(6-(diethylamino)-1-(2-((prop-2-yn-1-yloxy)carbonyl)phenyl)-3H-xanthen-3-ylidene)-N-ethylethanaminium) monocarbonate (AlRhod).

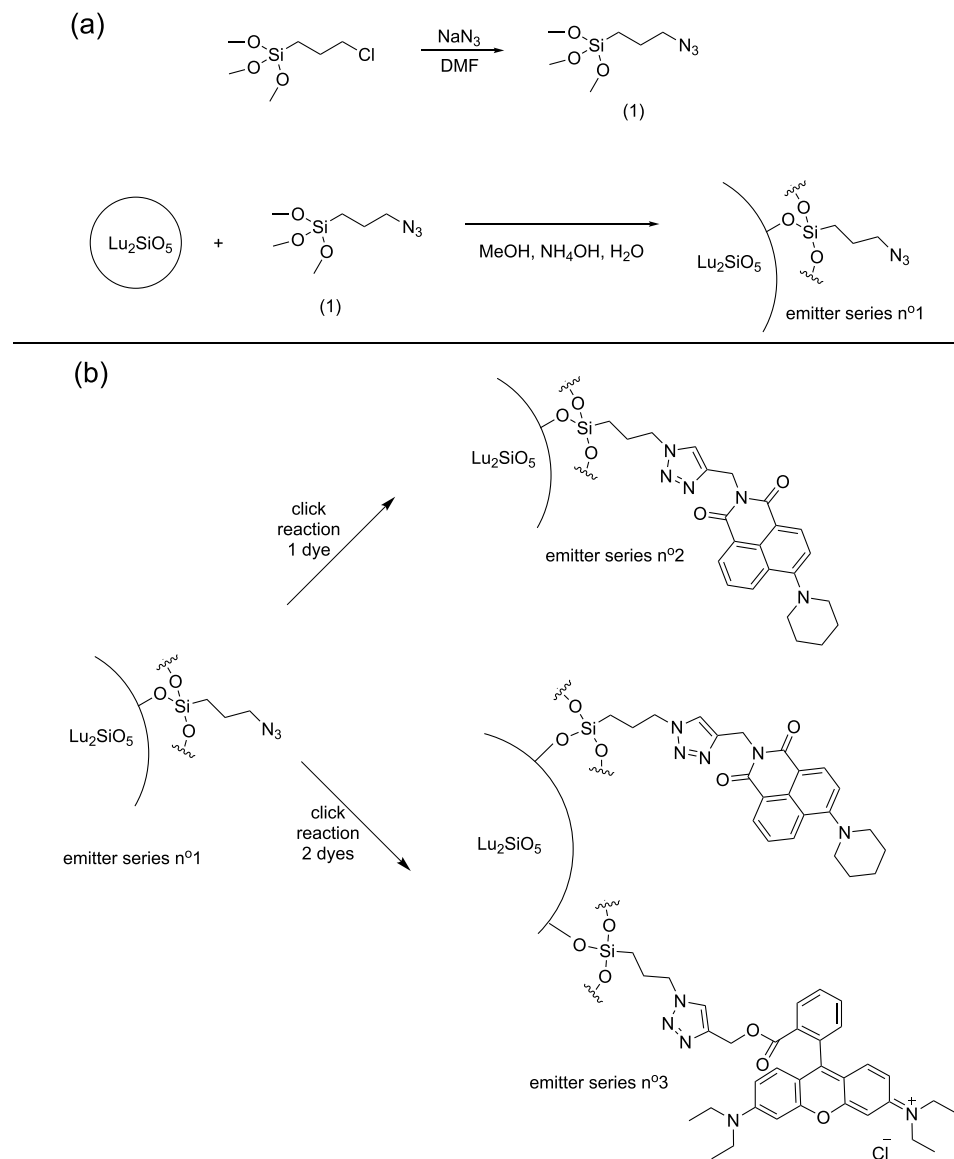


Figure 3. (a) Synthetic scheme to yield azide modified LSO:Ce particles. (b) Subsequent CuAAC reactions with either AlNap (1 dye) or AlNap and AlRhod (2 dyes).

performed via centrifugation at 27 216g for 15 min (cf. Figure 3b). Once the supernatant of emitter series 2 showed no peaks indicative of AlNap in the absorbance spectrum, emitter series 2 was said to be free from any unattached fluorophore. After the purification process, Fourier Transform Infrared (FTIR) spectroscopy of AlNap was compared to that of emitter series 2 to ensure attachment. The vigorous washing procedure and the subsequent FTIR, which confirms the presence of AlNap, suggests that a successful CuAAC

reaction does take place and that the AlNap is covalently attached to the LSO:Ce core (cf. Supporting Information).

Synthesis of Emitter Series 3. The synthesis of emitter series 3 was performed by utilizing a standard CuAAC reaction. Emitter series 1 (300 mg) was dispersed in THF (2 mL) and added to the reaction vessel. Then AlNap (5 mg, 0.016 mmol) in THF (1 mL) was added to the reaction mixture. Finally, copper(II) sulfate (39.14 mg, 0.157 mmol) in DI-water (1 mL) and sodium ascorbate (77.63 mg, 0.392 mmol) in DI-water (1 mL) were added to the reaction vessel. Then

the reaction vessel was placed in the J-KEM mini-reactor with stirring at 28 °C in the dark with a nitrogen purge. The reaction was allowed to proceed for 1 h. Then AlRhod (35 mg, 0.073 mmol) in THF (2 mL) was added to the reaction vessel. The reaction was allowed to proceed for an additional 24 h. Upon reaction completion, the product was washed with a 60:40 THF:water solution to remove the copper catalyst. Finally, the product was washed seven more times with THF. Washes were performed to remove any unattached dye from the particles. All washes were performed via centrifugation at 27 216g for 15 min (cf. Figure 3b). Once the supernatant of emitter series 3 showed no peaks indicative of either AlNap or AlRhod in the absorbance spectrum, emitter series 3 was said to be free from any unattached fluorophore. After the purification process, FTIR of AlRhod was compared to that of emitter series 3 as well as emitter series 2 to ensure attachment of both AlRhod and AlNap. The vigorous washing procedure and the subsequent FTIR, which confirms the presence of AlNap and AlRhod, suggests that a successful CuAAC reaction does take place and that the fluorophores are covalently attached to the LSO:Ce core (cf. Supporting Information).

Optical and X-ray Radioluminescence Characterization Methods.

Absorbance spectra were taken using a PerkinElmer Lambda 950 spectrophotometer. Photoluminescence spectra were collected using a Jobin-Yvon Fluorolog 3-222 Tau spectrometer. X-ray radioluminescence spectra were collected by irradiating the sample with a mini X-ray tube (Amptek Inc.), operating at a tube voltage of 50 kV and a tube current of 79 μ A. The radioluminescence was collected with a fiber bundle (Oriel) coupled to a MicroHR (Horiba Jobin Yvon) monochromator (spectral dispersion 5.25 nm/mm with spectral resolution of 0.25 nm) and a cooled CCD detector (Synapse, Horiba Jobin Yvon). The signal was collected on a grating with 600 line/mm and a blaze of 500 nm. The spectra were analyzed with SynerJY (Horiba Jobin Yvon) software. The exposure time varied from 1.2 to 20 s based on sample size and relative luminescence. Spectra were not corrected for the spectra sensitivity of the system.

Infrared Spectroscopy. Fourier transform infrared spectroscopy (FTIR) spectra were obtained on a ThermoScientific Nicolet 6700 FTIR instrument with a diamond crystal equipped with an attenuated total reflectance (ATR) attachment. Spectra were corrected for the ATR attachment and were baseline corrected prior to analysis. Analyses were performed with Omnic software.

Microscope Imaging. Microscope images were acquired on a Nikon Diaphot 300 inverted microscope with camera using OpenLab 3.1.4 software. Neuronal cell cultures were imaged using a 40 \times objective. Particles were added to the cell cultures using a pipet. Bright-field images were obtained of the cells and particles in the absence of X-ray excitation. Dark-field images of the radioluminescing particles were obtained by continually exciting the particles during a 4 min exposure with an Amptek mini-X X-ray unit (tube voltage of 40 kV and a tube current of 99 μ A) placed approximately 2 mm from the cell culture in a dark room. Dark-field images of the ambient background light were obtained the same as the radioluminescing particle images without any X-ray stimulation. Images were processed using MATLAB R2014b software. First, the ambient background image was subtracted from the radioluminescing particle image to remove any light not derived from the radioluminescence. Next, the background-subtracted radioluminescence image was contrast-enhanced such that 1% of the data was saturated at the high and low intensities of the image. This contrast-enhanced background-subtracted radioluminescence image was tinted green to accentuate the radioluminescence. Finally, the green-tinted image was overlaid on the bright-field image at 20% transparency.

Cultured Cortical Neurons. Approval was obtained for all experimental protocols from the University of Alabama at Birmingham Institutional Animal Care and Use Committee. All experiments were conducted in accordance with the Guide for the Care and Use of Laboratory Animals adopted by the U.S. National Institute of Health. Primary rat cortical neuronal cultures were obtained from embryonic day 18 rats as previously described.²⁸ Briefly, the cell culture coverslips were coated with poly-L-lysine (50

μ g/mL) overnight at 37 °C and then rinsed three times with autoclaved distilled water. Dissected cortical tissue was incubated with papain for 20 min at 37 °C. After rinsing in Hank's balanced salt solution, a single-cell suspension of the tissue was resuspended in Neurobasal media (Invitrogen) by trituration through a series of large to small fire-polished Pasteur pipets. Primary neuronal cells passed through a 70 μ M cell strainer were plated on poly-L-lysine coated coverslips in a 12 well plate. Cells were grown in Neurobasal media plus B-27 and L-glutamine supplement (complete Neurobasal media) for 15–16 days *in vitro* in a humidified CO₂ (5%) incubator at 37 °C. A 50% media change occurred weekly.

TUNEL Assay. The cortical neurons were incubated up to 24 h with ca. 800 nm azLSO/AlNap nanoparticles (final concentration 0.2–0.4 mg/mL) to determine effects on cell health. The nanoparticles were diluted in phosphate buffer saline (PBS), and a small volume (10–20 μ L) was added to the wells to prevent any changes in osmolarity. Cell death of primary cortical cultures was assessed using the TUNEL assay technique by the NeuroTACS *in situ* apoptosis detection kit (R&D Systems). After a brief rinse with PBS, coverslips were treated with 4% paraformaldehyde for 45 min. The rest of the procedure followed the recommended steps as indicated by the manufacturer to detect DNA fragments using the terminal deoxynucleotidyl transferase enzyme (TdT) and revealed through a horseradish peroxidase system. Positive and negative controls were performed. For the positive control, coverslips were treated with TACS-Nuclease (R&D Systems) that generates DNA breaks and showed a pale brown staining in the majority of the cells (>95%). No labeling was observed when TdT was not included in the reaction. Neuronal cells were counterstained with either DAPI (4'-6-diamidino-2-phenylindole) or Blue Counterstain (R&D Systems). Three to four coverslips were used for each condition. Multiple images (6–8) were taken and analyzed from each coverslip on an Olympus BX53 (40 \times objective) microscope. Visibility of neurons was reduced at the center of the application site due to the high concentration of nanoparticles; therefore images were taken in slightly less dense areas to improve visualization of the neurons and determine their survival. The cells were analyzed blind to the incubation period by two separate individuals, and the results were averaged together. All TUNEL analysis statistics were performed using Origin software (Origin Lab Corporation, 2002), and statistical significance was $P < 0.05$. Data are presented as means \pm SE, and sample number (n) refers to coverslips for TUNEL assay. Statistical comparisons were made using one-way ANOVA followed by Tukey's post hoc analysis.

Cultured Normal Human Dermal Fibroblast (NHDF) Cells. Normal human dermal fibroblast (NHDF) cells were obtained from ATCC. The NHDF cells were cultured in Dulbecco's modified Eagle's media (DMEM) containing 2% fetal bovine serum (FBS), 7.5 mM L-glutamine, 5 ng/mL rh FGF basic, 5 μ g/mL rh insulin, 1 μ g/mL hydrocortisone, and 50 μ g/mL ascorbic acid. Cells were cultured at 37 °C in a humidified atmosphere of 95% air/5% CO₂.

MTS Assay. Normal human dermal fibroblast (NHDF) cells were plated in 96 well plates at a cell density of 7000 cells per well. After the cells were plated for 24 h, the cells were incubated with ca. 800 nm commercial LSO:Ce particulates in concentrations of 3.6×10^7 , 3.6×10^8 , or 3.6×10^9 particles/mL. At each concentration, the cells were incubated for 24, 48, or 72 h. At the conclusion of each time point, the cell viability was measured using a [3-(4,5-dimethylthiazol-2-yl)-5-(3-carboxymethoxyphenyl)-2-(4-sulfophenyl)-2H-tetrazolium, inner salt (MTS) assay (CellTiter 96 AQ_{ueous} One Solution Cell Proliferation Assay, Promega, Fitchburg, WI) following the manufacturer's protocol. Briefly, the media was removed, and the plate was washed several times with phosphate buffered saline (PBS) before adding a solution containing 200 μ L of DMEM media and 40 μ L of the MTS assay reagent. After 3 h, the absorbance was measured using a plate reader at OD = 490 nm.

Thermal Characterization Methods. Thermogravimetric analysis (TGA) was performed on a TA Instruments Hi-Res TGA 2950 thermogravimetric analyzer equipped with Universal Analysis software. All TGAs were performed from room temperature to 1000 °C at 10 °C/min in a nitrogen atmosphere with a switch to air at

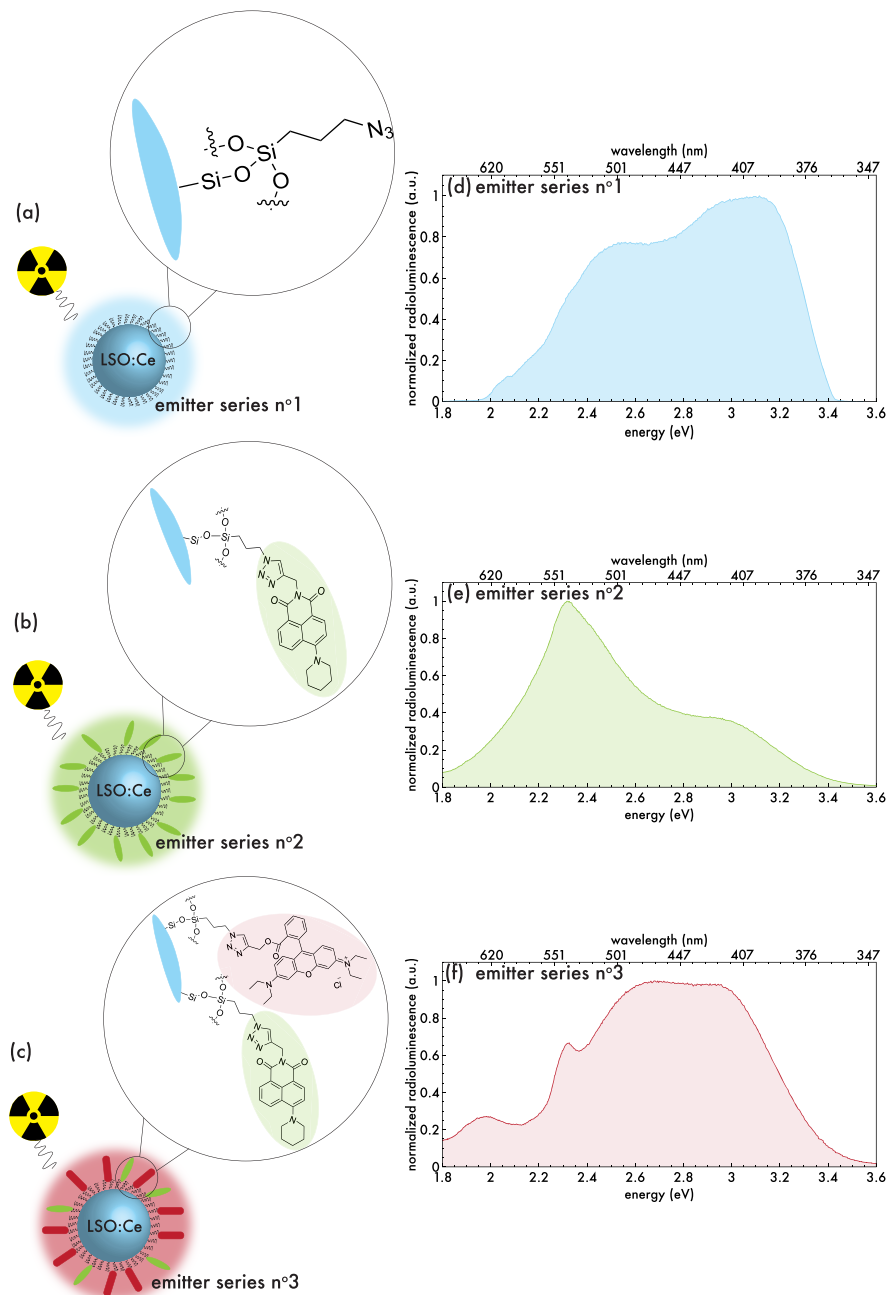


Figure 4. (a) Lutetium oxyorthosilicate doped with cerium (LSO:Ce) particles of median size ca. 800 nm surface modified with 3-azidopropyl(trimethoxy)silane (emitter series 1), which emit blue when excited with X-rays. (b) Emitter series 1 surface modified with 6-piperidin-1-yl-2-prop-2-yn-1-yl-1H-benzo[de]isoquinoline-1,3-(2H)-dione (AlNap) with a CuAAC transformation (emitter series 2); emitter series 2 emits green upon X-ray irradiation. (c) Emitter series 1 surface modified with AlNap and N-(6-diethylamino)-9-{2-[(prop-2-yn-1-yl-1H-benzo[de]isoquinoline-1,3-(2H)-dione)-3H-xanthene-3-ylidene]-N-ethylethanaminium (AlRhod) with multiple CuAAC reactions; emitter series 3 emits elements of red, green, and blue upon X-ray irradiation. X-ray radioluminescence spectra of (d) emitter series 1, (e) emitter series 2, and (f) emitter series 3. X-ray radioluminescence spectra obtained with an AmpTek Mini-X instrument equipped with a silver target operating at 50 kV and 79 μ A.

700 °C. Before each TGA run, the sample was purged in the furnace with nitrogen for 15 min. Thermogravimetric analysis was performed on particulate systems to determine fluorophore or silane ligand coverage of the particles.

Scanning Electron Microscopy. A Hitachi 4800 field emission scanning electron microscope (FE-SEM) was used to obtain size distribution of azLSO:Ce. The samples were platinum coated at 15 mA for 1 min under argon conditions at 200 mTorr. Images of secondary electrons were taken with an accelerating voltage of 15 kV. Image analysis was performed using ImageJ software, and dimensions were calibrated according to the scale bar of each picture.

RESULTS AND DISCUSSION

In the current effort, ca. 800 nm commercial lutetium oxyorthosilicate doped with cerium (LSO:Ce) phosphors containing 1–10 atom % cerium, as specified by the manufacturer, were surface modified through organometallic chemistry with a silane linker (cf. Figure 4a, emitter series 1) to enable subsequent copper(I) catalyzed azide/alkyne cycloaddition (CuAAC) reactions. Through CuAAC reactions between emitter series 1 and 6-piperidin-1-yl-2-prop-2-yn-1-yl-1H-benzo[de]isoquinoline-1,3-(2H)-dione (cf. Figure 4b,

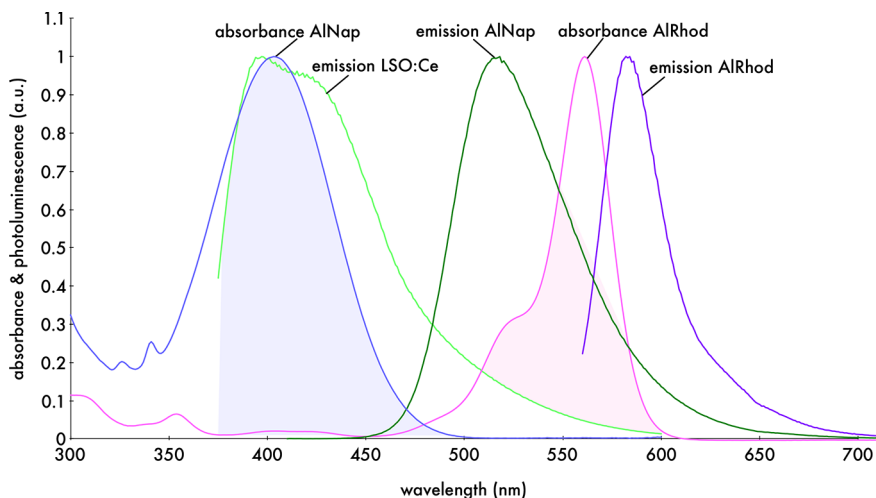


Figure 5. (a) Absorbance of 6-piperidin-1-yl-2-prop-2-yn-1-yl-1*H*-benzo[*de*]isoquinoline-1,3-(2*H*)-dione (AlNap), optical emission of LSO:Ce (light green), optical emission of AlNap (dark green), absorbance of *N*-(6-diethylamino)-9-{2-[(prop-2-yn-1-yloxy)carbonyl]phenyl}-3*H*-xanthan-3-ylidene)-*N*-ethylethanaminium (AlRhod) (pink), and optical emission of AlRhod (purple). Shaded are the areas of emission/absorbance overlap. Excitation of LSO:Ce, AlNap, and AlRhod at 357, 400, and 550 nm, respectively. All concentrations were 5 μ g/mL with the exception of LSO, which was measured in its solid form.

emitter series 2) and *N*-(6-diethylamino)-9-{2-[(prop-2-yn-1-yloxy)carbonyl]phenyl}-3*H*-xanthan-3-ylidene)-*N*-ethylethanaminium (cf. Figure 4c, emitter series 3), the X-ray radioluminescence of LSO:Ce could be transformed from its normal blue emission (cf. Figure 4d) to have elements of green (cf. Figure 4e, emitter series 2) and red (cf. Figure 4f, emitter series 3) in the X-ray radioluminescence spectra through Förster Resonance Energy Transfer (FRET).

Photophysics of Fluorophores. The 6-piperidin-1-yl-2-prop-2-yn-1-yl-1*H*-benzo[*de*]isoquinoline-1,3-(2*H*)-dione (AlNap) has an absorbance at 400 nm.^{29,30} The emission profile of AlNap exhibits a maximum emission at ca. 515 nm.^{26,31,32} The maximum absorbance of *N*-(6-diethylamino)-9-{2-[(prop-2-yn-1-yloxy)carbonyl]phenyl}-3*H*-xanthan-3-ylidene)-*N*-ethylethanaminium (AlRhod) was ca. 550 nm with an aggregation peak at 515 nm, while the maximum emission for AlRhod was ca. 585 nm when excited at 550 nm (cf. Figure 5).^{33–35} No significant emission was detected for the naphthalimide and rhodamine B derivatives when irradiated with X-rays (data not shown). It is obvious that the emission of LSO:Ce overlaps well with AlNap, and the emission of AlNap overlaps well with the absorbance of AlRhod.

Surface Modification of LSO:Ce. Polycrystalline ceramic LSO:Ce contains lutetium, silicon, oxygen, and a small percentage of doped cerium atoms that occupy lutetium sites. The LSO:Ce particles are modified by attaching an organometallic linker with an azide group on one end ((3-azidopropyl)(trimethoxy)silane) to the particle via a base catalyzed hydrolysis reaction in the presence of ammonium hydroxide in a methanol solution. Upon a basic aqueous environment the methoxy groups on the end of the linker hydrolyze to alcohol groups, which readily react with the surface of the LSO:Ce particle by forming Si–O–Si bonds (cf. Figure 4a, emitter series 1).^{36,37} At the completion of the reaction, the product was put through a vigorous washing (through centrifugation) purification process with a good solvent for the silane linker to remove any unattached linker. While surfaces of larger particles are less energetic, longer reaction times do result in modification; Fourier transform infrared spectroscopy (FTIR) confirmed attachment of the

azide linker as indicated by the peak at 2100 cm^{-1} , which is related to the stretching of the N=N (cf. Supporting Information). In this way, azide modified LSO:Ce (azLSO:Ce) particles are able to undergo a variety of CuAAC reactions, where a variety of fluorescent tags, proteins, and targeting moieties could be covalently attached to the particles to enhance their utility in bioimaging or other therapies.³⁸ Therefore, non-hygroscopic LSO:Ce can easily be surface modified via facile reactions to exhibit emissions that cover the visible spectrum.

X-ray Radioluminescence of Fluorophore Modified LSO:Ce. Upon X-ray irradiation, the cerium dopant in the LSO crystal structure causes LSO:Ce to emit in the blue portion of the visible spectrum. Before any modifications were performed, X-ray radioluminescence was obtained for the commercial LSO:Ce particles as a control. X-ray radioluminescence spectrum of the as received, commercial LSO:Ce particles (size 2–4 μm) was deconvoluted into three peaks at 396 nm (3.13 eV), 428 nm (2.90 eV), and 498 nm (2.49 eV) (cf. Figure 6). Ce³⁺ resides in two distinct crystallographic sites with the first site (Ce1 site) being the 6-oxygen-coordinated site and the second site (Ce2 site) being the 7-oxygen-coordinated site, where the Ce1 site is the dominant site in X-ray radioluminescence.³⁹ Particles of 2–4 μm are too large to be successful bioimaging agents; therefore, the as received particles were ball milled in ethanol to achieve a median particle size of 800 nm, which is a more viable size for bioimaging agents (cf. Figure 7). Three SEM micrographs at varying magnifications are presented to show detail of the particles post-ballmilling. The ball milled ca. 800 nm LSO:Ce particles were used in all further processes.

In emitter series 1, the deconvolution of the X-ray radioluminescence spectrum revealed 2 peaks at 397 nm (3.12 eV) and 428 nm (2.90 eV) resulting from the Ce1 site. In each crystallographic site there are two 4f ground states ($^2\text{F}_{5/2}$ (emission at higher energy) and $^2\text{F}_{7/2}$ (emission at lower energy)) due to spin orbit coupling.^{40–42} There is a shoulder at ca. 498 nm (2.48 eV) resulting from the combination of both 4f states in the Ce2 site (cf. Figure 8a), which agrees well with the energy profile for commercially available LSO:Ce

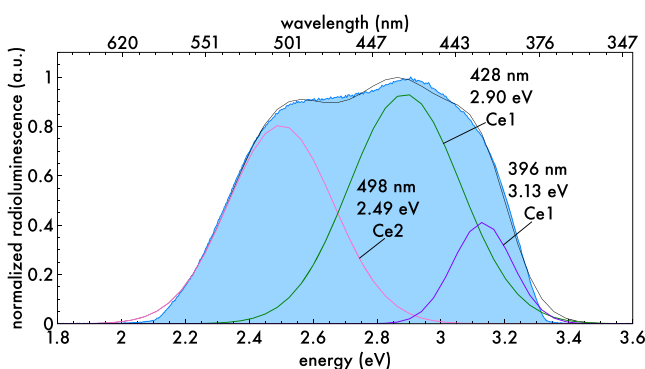


Figure 6. Deconvolution of the X-ray radioluminescence spectrum of commercial, as received LSO:Ce particles ($2\text{--}4\ \mu\text{m}$). Deconvolutions revealed peaks at 498 nm (pink, attributed to the Ce2 site), 428 nm, and 396 nm (green and purple, respectively, both attributed to the Ce1 site). X-ray radioluminescence spectra obtained with an AmpTek Mini-X instrument equipped with a silver target operating at 50 kV and 79 μA .

polycrystalline ceramics. The slight difference in the shape of the energy profile and shifted deconvoluted peaks, when compared to commercial LSO:Ce, can be due to the surface modification of emitter series 1 since the emission of Ce^{3+} is greatly influenced by its environment due to the unshielded $4f \rightarrow 5d$ transition.⁴³ While the Ce^{3+} on the inside of the particle would not be influenced by the silane linker on the surface, the Ce^{3+} close to the surface of the particle may feel the effects of the ligand, leading to a slight shift in the energy profile. Additionally, the overall size of emitter series 1 is smaller when compared to commercial LSO:Ce, which can influence the energy profile^{44,45} though clearly none of these modifications had a great influence on the X-ray radioluminescent emission characteristics of LSO:Ce. The emission of emitter series 1 could be tuned via judicious choice of FRET pairs. By utilizing LSO:Ce as the X-ray excited “pump” source for other non-X-ray active fluorophores, the emission of the particles could be tuned to range the entire visible spectrum on the basis of a blue emitter.

The 6-piperidin-1-yl-2-prop-2-yn-1-yl-1H-benzo[*de*]-isoquinoline-1,3-(2*H*)-dione (AlNap), when covalently attached to the surface of emitter series 1, forms a FRET pair with LSO:Ce (cf. Figure 4b, emitter series 2), causing an X-ray emission shift from blue (dominate peak at ca. 420 nm) to green (dominant peak at ca. 525 nm) (cf. Figure 4e). It is clear from the deconvoluted radioluminescence spectrum of emitter series 2 that a significant portion of the energy from LSO:Ce has been transferred to AlNap as indicated by the appearance of the peaks at ca. 525 nm (2.36 eV) and 534 nm (2.32 eV), which are attributed to the monomeric and J-aggregate peaks,

respectively, of AlNap as these peaks coincide well with the peaks observed in the photoluminescence spectrum of AlNap.^{26,31,32} The Förster distance (i.e., the distance at which FRET is 50% efficient) between LSO:Ce and AlNap is ca. 2.98 nm when 0.30 is used as the quantum efficiency of LSO:Ce;⁴⁶ it should be noted that energy contributing to FRET is only considered from the surface of the LSO:Ce core. With this in mind, upon modeling AlNap as a sphere of diameter 1.4 nm, which is the fully extended length of the dye, 0.405 nm³ is directly in contact with the surface of the LSO:Ce particle, which indicates that FRET is a possibility. Furthermore, the volume of the sphere representative of the dye is 1.44 nm³, and if we look at Förster distance as a volume, which is 9 nm³, the Förster “volume” is 6.27 times larger than the volume of the fluorophore. While the existence of photon emission and photon reabsorbance cannot be completely obviated, there is strong evidence to suggest that FRET is a viable energy transfer mechanism. This type of behavior is expected for all systems reported.

The deconvolution of emitter series 2 revealed only one LSO:Ce peak at 413 nm (3.00 eV); this is likely a combination of the peaks at 397 nm (3.12 eV) and 428 nm (2.90 eV) found in the spectrum of emitter series 1, as 413 nm (3.00 eV) is the average of these two peaks (cf. Figure 8b). Additionally, the band relating to the Ce2 site could not be deconvoluted as it overlaps heavily with the strong AlNap bands; efforts to introduce additional peaks in the deconvolution of the spectrum in Figure 8b do not provide changes in the fitting curve, as the fitting software attempted to minimize the influence of those peaks. This can indicate that some of the peaks present in Figure 8a could merge together or be suppressed in Figure 8b due to the introduced energy transfers caused by AlNap. Based on the ratio of the integral of the AlNap component of the X-ray radioluminescence spectrum to the total integral of the spectrum, the dye component is responsible for 78% of the total spectrum suggesting that energy transfer is efficient. In emitter series 3 (cf. Figure 4c), LSO:Ce and AlNap remain FRET pairs with one another, but AlNap then transfers its energy to *N*-(6-diethylamino)-9-{2-[(prop-2-yn-1-yloxy)carbonyl]phenyl}-3*H*-xanthen-3-ylidene)-*N*-ethylethanaminium (AlRhod) through an additional FRET, resulting in a shift from a blue emission to a blue emission with a prominent green and red component (cf. Figure 4f). The Förster distance between AlNap and AlRhod is ca. 3.62 nm. When comparing the integral of the AlRhod component of the X-ray radioluminescence spectrum to the total spectrum, the AlRhod component composes 10.5% of the total X-ray radioluminescence spectrum.

The deconvolution of the radioluminescence spectra of emitter series 3 revealed an AlRhod peak at 633 nm (1.96 eV),

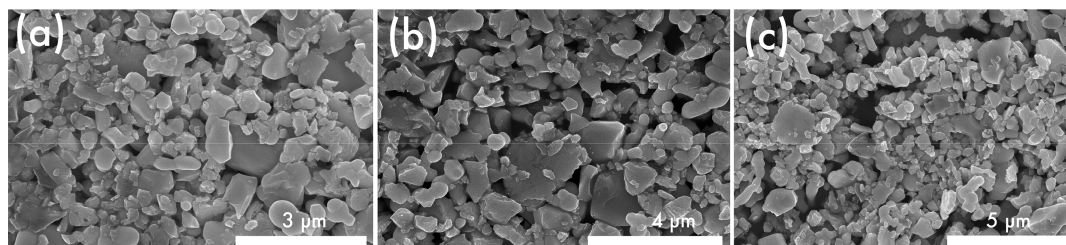


Figure 7. Scanning electron micrographs (SEM) of LSO:Ce particles (median size 800 nm) at a magnification of (a) 9000 (scale bar 3.00 μm), (b) 12 000 (scale bar 4.00 μm), and (c) 15 000 (scale bar 5.00 μm). Images were taken at 15 kV and 10 μA .

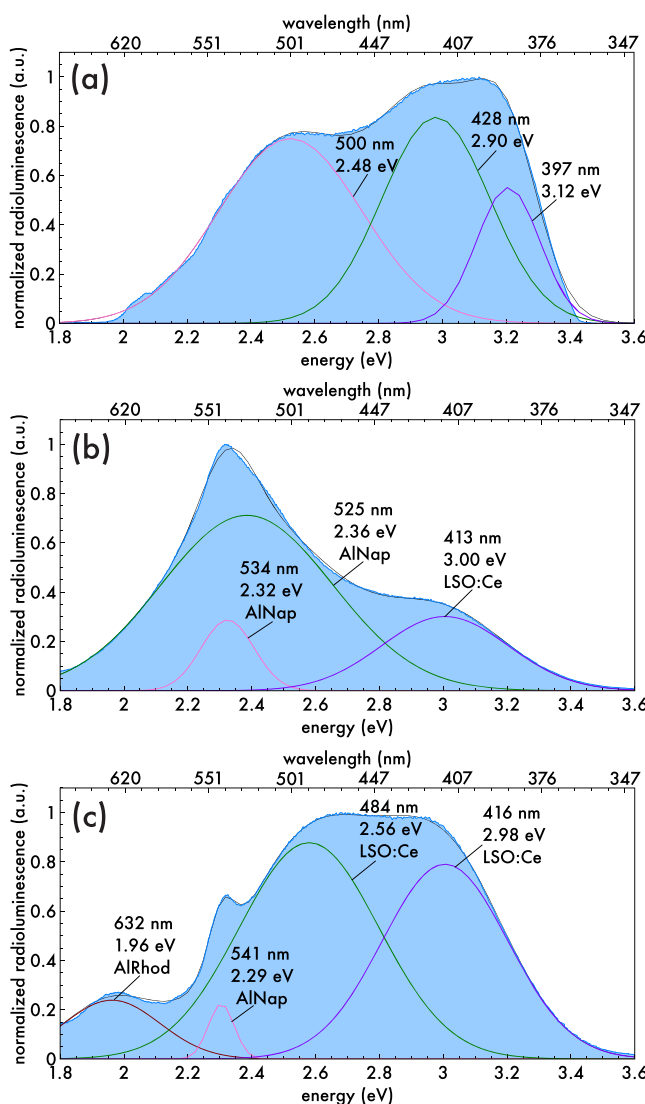


Figure 8. Deconvolution of the radioluminescence spectrum of (a) emitter series 1 revealed 3 peaks at 397 nm (3.12 eV), 428 nm (2.90 eV), and 500 nm (2.48 eV), which corresponds to Ce^{3+} , $^2\text{F}_{5/2}$, and $^2\text{F}_{7/2}$ in the first crystallographic site and a combination of the 4f states in the second crystallographic site, respectively. (b) Emitter series 2 showed AlNap with an aggregate peak at 534 nm (2.32 eV) and a monomeric peak at 525 nm (2.36 eV) as well as an LSO:Ce peak at 413 nm (3.00 eV), which is a combination of the 397 nm (3.12 eV) and 428 nm (2.90 eV) peak observed in emitter series 1. (c) Emitter series 3 exhibited an aggregate AlRhod peak at 633 nm (1.96 eV), a peak at 541 nm (2.29 eV) which is a combination of the monomeric AlRhod peak and AlNap peaks, and two LSO:Ce peaks at 484 nm (2.56 eV) and 416 nm (2.98 eV), which are slightly blue-shifted from the expected peaks. Total fit for the deconvolutions is presented in black with the actual data presented in blue. All X-ray radioluminescence spectra were obtained with an AmpTek Mini-X instrument equipped with a silver target operating at 50 kV and 79 μA .

which coincides well with the photoluminescence J-aggregate peak of rhodamine B. There is also a peak at 541 nm (2.29 eV), which is likely a combination of a small monomeric AlRhod peak, which should be at ca. 585 nm (2.12 eV) with a major contribution from AlNap as this peak is slightly red-shifted from the expected AlNap peak at ca. 525 nm (2.36 eV). Clearly, the energy transfers that takes place with emitter series

3 are not as good as emitter series 2, as two LSO:Ce bands could easily be deconvoluted; however, these bands are red-shifted from their expected peaks at 397 nm (3.12 eV) and 428 nm (2.90 eV) which suggests that the peak from the Ce2 site is embedded in the two LSO:Ce peaks observed in Figure 8c. To maintain the fit, the peak attributed to the Ce2 site could not be deconvoluted separately from the presented LSO:Ce peaks. Both AlNap and AlRhod are stable against X-ray irradiation as the fluorophores were exposed to several cycles of X-ray irradiation with photoluminescence of each fluorophore being obtained after each radiation cycle. The photoluminescence spectra of AlNap and AlRhod did not change at any time after exposure to X-ray radiation (data not shown), indicating that the molecular structure of the fluorophores remained intact as photoluminescence of the molecules would change upon bond destruction.

Neuronal Assessment with Particulate Systems. It is clear from the radioluminescence spectra of emitter series 2 and 3 that X-ray radiation can induce FRET between an X-ray active pump source and non-X-ray active fluorophores. Therefore, these particles have potential as imaging agents for deep tissue applications. To evaluate their imaging ability, emitter series 2 was incubated with cultured single-cell layer rat cortical neurons and imaged (cf. Figure 9). Upon being in a water-rich, biological environment, emitter series 2, which was a mix of a nonactive precursor compound and ca. 10% AlNap, was imaged under X-ray irradiation using a standard photomicrography microscope. However, even with AlNap in low yield, emitter series 2 was still able to be imaged under physiological conditions. This is a good indication that the particles are not degraded in an aqueous environment.^{47,48} Furthermore, control studies of neurons incubated with particles but without X-ray irradiation showed only a black picture (data not shown). While the particles were able to be successfully imaged, we needed to ensure that the particles did not induce any cytotoxicity. Because emitter series 2 was imaged with rat cortical neurons, the terminal deoxynucleotidyl transferase dUTP nick end labeling (TUNEL) toxicity assay was also performed with rat cortical neurons. Primary cortical neurons are particularly sensitive to slight alterations in their culturing conditions, which can lead to their cell death.⁴⁹ Cell death involves atrophy of the cell body, condensation of the nuclear chromatin, DNA fragmentation, and neurite degeneration. A TUNEL assay was used to determine the number of neurons that had undergone cell death for each condition (cf. Figure 10a). The presence of 1.01×10^{11} particles/mL or 2.02×10^{11} particles/mL of emitter series 2 did not decrease the number of viable cells in culture at the various time points observed (cf. Figure 10b). Additionally, there was no change in the neuronal density between the various conditions (cf. Figure 10c). While emitter series 2 did not exhibit any cytotoxicity, it needed to be ensured that unmodified LSO:Ce particles did not induce cytotoxicity. Therefore, LSO:Ce particles were incubated with normal human dermal fibroblasts for 24, 48, and 72 h at particle concentrations of 3.6×10^7 , 3.6×10^8 , or 3.6×10^9 particles/mL. At all concentrations and at all time points, there was no observable cytotoxicity as confirmed via a 3-(4,5-dimethylthiazol-2-yl)-5-(3-carboxymethoxyphenyl)-2-(4-sulfophenyl)-2H-tetrazolium (MTS) assay statistically analyzed with Tukey's test (cf. Figure 10d). As the particles do not induce cytotoxicity, these particles are potential viable bioimaging agents.

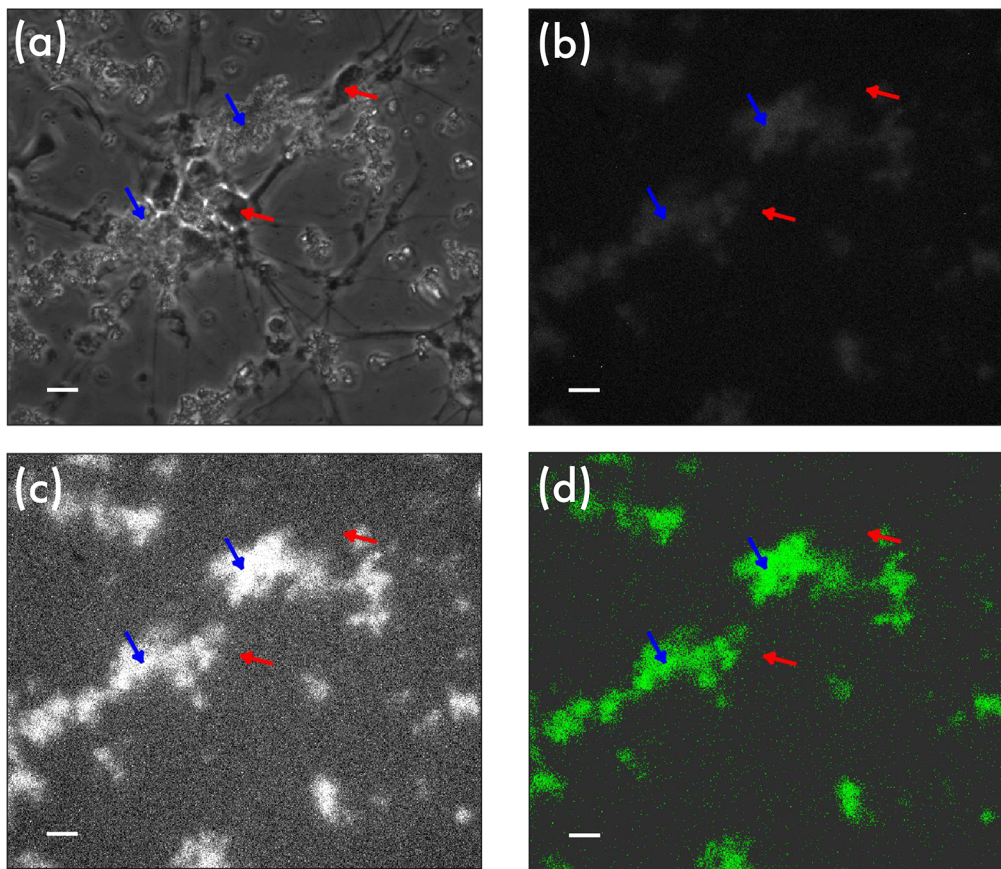


Figure 9. Microscopy images of neurons with emitter series 2 in culture. Neurons and particles imaged in (a) bright-field, (b) under X-ray irradiation with background subtraction in dark-field, (c) under X-ray irradiation with contrast enhancement under X-ray irradiation with background subtraction, and (d) under X-ray irradiation with contrast enhancement under X-ray irradiation with background subtraction pseudocolored green. All scale bars are 50 μ m. X-ray irradiation performed with an AmpTek Mini-X instrument equipped with a silver target operating at 40 kV and 99 μ A. Blue arrows indicate the soma of the neurons, while red arrows indicate emitter series 2.

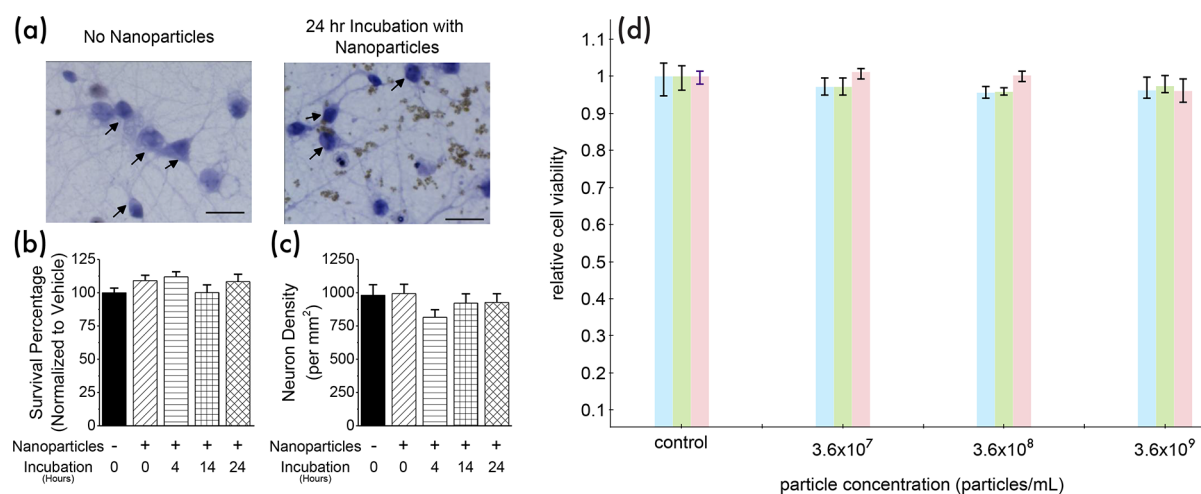


Figure 10. Cultured cortical neurons were incubated for up to 24 h with or without emitter series 2. The cells were then fixed, analyzed for TUNEL reactivity, and counterstained blue to visualize the neurons. (a) Images of cortical neurons with and without emitter series 2 after processing with the TUNEL assay. The black arrows indicate examples of healthy neurons. Dead neurons were identified as cells that showed TUNEL reactivity through the brown staining of the condensed chromatin. Scale bar 25 μ m. (b) Group data show no change in neuronal survival at any of the incubation time points (0, 4, 14, and 24 h) (ANOVA, $F_{4,108} = 1.2$, $P = 0.31$, $n = 3, 3, 3, 3, 4$). Six to eight images from each coverslip were analyzed. (c) The overall neuronal density was unchanged (ANOVA, $F_{4,108} = 1.0$, $P = 0.39$, $n = 3, 3, 3, 3, 4$). (d) MTS cytotoxicity assay of normal human dermal fibroblast (NHDF) cell incubated without particles (control) or with 3.6×10^7 , 3.6×10^8 , or 3.6×10^9 particles/mL for 24 h (blue), 48 h (green), and 72 h (pink). No cytotoxicity was observed for any of the concentrations at any time point as analyzed by Tukey's test.

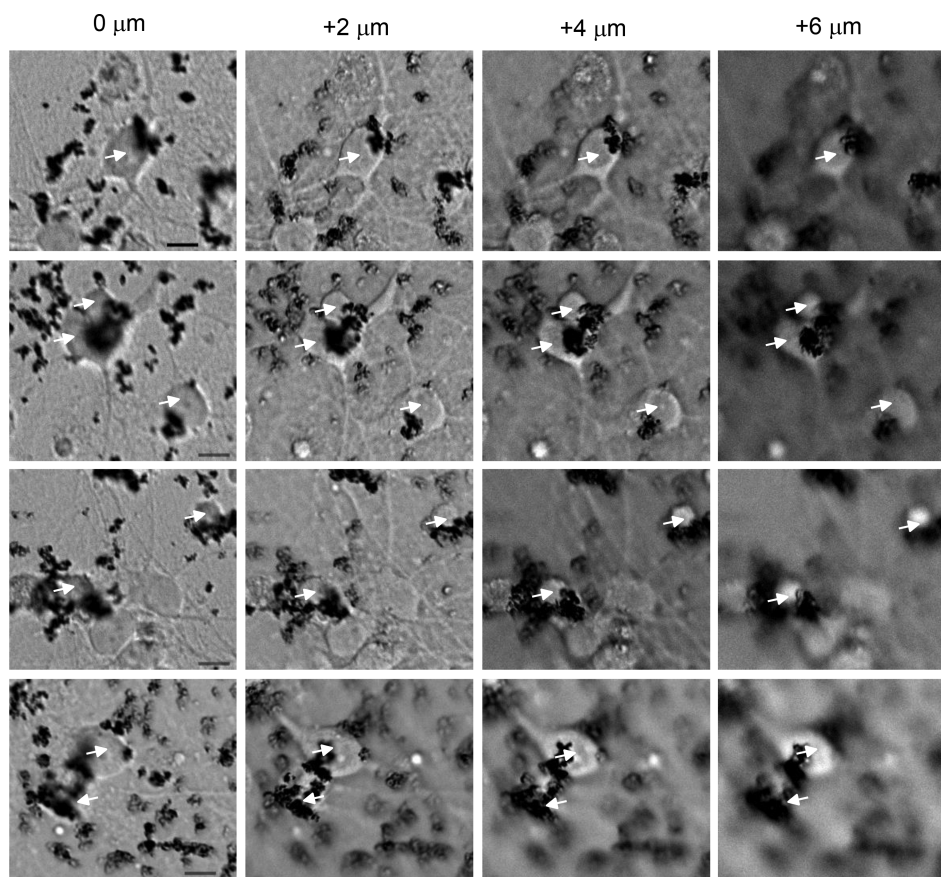


Figure 11. Cultured cortical neurons were incubated for 24 h with nanoparticles. Each row is a z-stack image separated by 2 μm . The white arrows indicate neurons with nanoparticles (small dark structures) sitting on top of the neurons. The nanoparticles come into focus on a slightly different plane than the neuronal cell bodies. All scale bars are 10 μm .

It was noticed that acute application of nanoparticles resulted in the nanoparticles quickly surrounding the cells. For applications involving proteins localized on the cellular membrane extracellularly, particle uptake by the cells can be undesirable.^{50,51} To assess the potential for neurons to engulf the imaging probes, neurons were incubated for 24 h with the nanoparticles, and then z-stack images were taken. Figure 11 shows that even after 24 h the nanoparticles are still sitting on the cell surface. Therefore, these particulate systems are suitable to extracellular bioimaging.

■ SUMMARY AND CONCLUSIONS

As X-ray bioimaging and theranostics continue to become more clinically viable options, the need for better, more versatile imaging agents will grow. Herein, we created a particulate system based in LSO:Ce cores that have been surface modified with green emitting (AlNap) and red emitting (AlRhod) to generate systems that are capable of emitting at a variety of colors when the core is excited with X-ray radiation. These particles were successfully imaged *in vitro* with rat cortical neurons. The particulate systems were tested for cytotoxicity with multiple assays and were never shown to be cytotoxic at high particle concentrations for up to 72 h. Additionally, due to the ease of surface functionalization of the particles, the particles could be functionalized to target various extracellular targets for robust bioimaging.

■ ASSOCIATED CONTENT

Supporting Information

The Supporting Information is available free of charge on the ACS Publications website at DOI: [10.1021/acs.langmuir.8b03129](https://doi.org/10.1021/acs.langmuir.8b03129).

FTIR spectra of emitter series 1, 2, and 3 ([PDF](#))

■ AUTHOR INFORMATION

Corresponding Author

*E-mail: foulger@clemson.edu. Phone: 01 864-656-1045. Fax: 01 864-656-1049.

ORCID

Stephen H. Foulger: [0000-0002-4221-2154](https://orcid.org/0000-0002-4221-2154)

Notes

The authors declare no competing financial interest.

■ ACKNOWLEDGMENTS

The authors wish to thank Dr. Jeremy Day (University of Alabama Birmingham) for providing the neuronal cultures. In addition, the authors wish to thank Nancy Gallus (Day group) for preparing the neurons. The authors thank the Gregg-Graniteville Foundation and the National Science Foundation (OIA-1632881) for financial support.

■ REFERENCES

(1) Chen, H. Y.; Rogalski, M. M.; Anker, J. N. Advances in functional X-ray imaging techniques and contrast agents. *Phys. Chem. Chem. Phys.* **2012**, *14*, 13469–13486.

(2) Lee, N.; Choi, S. H.; Hyeon, T. Nano-Sized CT Contrast Agents. *Adv. Mater.* **2013**, *25*, 2641–2660.

(3) Hounsfield, G. N. Computerized transverse axial scanning tomography 0.1. Description of system. *Br. J. Radiol.* **1973**, *46*, 1016–1022.

(4) Pereira, G. R.; Rocha, H. S.; Calza, C.; Anjos, M. J.; Lima, I.; Perez, C. A.; Lopes, R. T. 3D elemental distribution images in biological samples by XRF mu CT. *X-Ray Spectrom.* **2011**, *40*, 260–264.

(5) Xue, Z. L.; Li, X. L.; Li, Y. B.; Jiang, M. Y.; Liu, H. R.; Zeng, S. J.; Hao, J. H. X-ray-Activated Near-Infrared Persistent Luminescent Probe for Deep-Tissue and Renewable in Vivo Bioimaging. *ACS Appl. Mater. Interfaces* **2017**, *9*, 22132–22142.

(6) Hu, Z. H.; Qu, Y. W.; Wang, K.; Zhang, X. J.; Zha, J. L.; Song, T. M.; Bao, C. P.; Liu, H. X.; Wang, Z. L.; Wang, J.; Liu, Z. Y.; Liu, H. F.; Tian, J. In vivo nanoparticle-mediated radiopharmaceutical-excited fluorescence molecular imaging. *Nat. Commun.* **2015**, *6*, 7560.

(7) Sudheendra, L.; Das, G. K.; Li, C. Q.; Stark, D.; Cena, J.; Cherry, S.; Kennedy, I. M. NaGdF4:Eu3+ Nanoparticles for Enhanced X-ray Excited Optical Imaging. *Chem. Mater.* **2014**, *26*, 1881–1888.

(8) Sun, C.; Pratx, G.; Carpenter, C. M.; Liu, H. G.; Cheng, Z.; Gambhir, S. S.; Xing, L. Synthesis and Radioluminescence of PEGylated Eu3+-doped Nanophosphors as Bioimaging Probes. *Adv. Mater.* **2011**, *23*, H195–H199.

(9) Bizarri, G. Scintillation mechanisms of inorganic materials: From crystal characteristics to scintillation properties. *J. Cryst. Growth* **2010**, *312*, 1213–1215.

(10) Nikl, M.; Laguta, V. V.; Vedda, A. Complex oxide scintillators: Material defects and scintillation performance. *Phys. Status Solidi B* **2008**, *245*, 1701–1722.

(11) Nikl, M.; Yoshikawa, A.; Kamada, K.; Nejedzchleb, K.; Stanek, C. R.; Mares, J. A.; Blazek, K. Development of LuAG-based scintillator crystals - A review. *Prog. Cryst. Growth Charact. Mater.* **2013**, *59*, 47–72.

(12) Pidol, L.; Guillot-Noel, O.; Kahn-Harari, A.; Viana, B.; Pelenc, D.; Gourier, D. EPR study of Ce3+ ions in lutetium silicate scintillators Lu2Si2O7Lu2SiO5. *J. Phys. Chem. Solids* **2006**, *67*, 643–650.

(13) Wojtowicz, A. J.; Glodo, J.; Drozdowski, W.; Przegietka, K. R. Electron traps and scintillation mechanism in YAlO3:Ce and LuAlO3:Ce scintillators. *J. Lumin.* **1998**, *79*, 275–291.

(14) Paik, T.; Gordon, T. R.; Prantner, A. M.; Yun, H.; Murray, C. B. Designing Tripodal and Triangular Gadolinium Oxide Nanoplates and Self-Assembled Nanofibrils as Potential Multimodal Bioimaging Probes. *ACS Nano* **2013**, *7*, 2850–2859.

(15) Carpenter, C. M.; Sun, C.; Pratx, G.; Rao, R.; Xing, L. Hybrid x-ray/optical luminescence imaging: Characterization of experimental conditions. *Med. Phys.* **2010**, *37*, 4011–4018.

(16) Guo, T.; Lin, Y.; Zhang, W. J.; Hong, J. S.; Lin, R. H.; Wu, X. P.; Li, J.; Lu, C. H.; Yang, H. H. High-efficiency X-ray luminescence in Eu3+-activated tungstate nanoprobes for optical imaging through energy transfer sensitization. *Nanoscale* **2018**, *10*, 1607–1612.

(17) Naczynski, D. J.; Sun, C.; Turkcan, S.; Jenkins, C.; Koh, A. L.; Ikeda, D.; Pratx, G.; Xing, L. X-ray-Induced Shortwave Infrared Biomedical Imaging Using RareEarth Nanoprobes. *Nano Lett.* **2015**, *15*, 96–102.

(18) Li, X. L.; Xue, Z. L.; Jiang, M. Y.; Li, Y. B.; Zeng, S. J.; Liu, H. R. Soft X-ray activated NaYF4:Gd/Tb scintillating nanorods for in vivo dual-modal X-ray/X-ray-induced optical bioimaging. *Nanoscale* **2018**, *10*, 342–350.

(19) Yen, W. M.; Weber, M. J. *Inorganic Phosphors: Compositions, Preparation and Optical Properties*; CRC Press LLC: Boca Raton, FL, 2004; p 456.

(20) Avdeichikov, V. V.; Bergholt, L.; Guttormsen, M.; Taylor, J. E.; Westerberg, L.; Jakobsson, B.; Klamra, W.; Murin, Y. A. Light output and energy resolution of CSI, YAG, GSO, BGO and LSO scintillators for light-ions. *Nucl. Instrum. Methods Phys. Res., Sect. A* **1994**, *349*, 216–224.

(21) Zhuravleva, M.; Stand, L.; Wei, H.; Hobbs, C.; Boatner, L. A.; Ramey, J. O.; Shah, K.; Burger, A.; Rowe, E.; Bhattacharya, P.; Tupitsyn, E.; Melcher, C. L.; 2013 IEEE Nuclear Science Symposium and Medical Imaging Conference; IEEE, 2013; pp 1–5.

(22) Chen, Q.; et al. All-inorganic perovskite nanocrystal scintillators. *Nature* **2018**, *S61*, 88–93.

(23) Wang, T.; Chirmanov, V.; Chiu, W. H. M.; Radovanovic, P. V. Generating Tunable White Light by Resonance Energy Transfer in Transparent Dye-Conjugated Metal Oxide Nanocrystals. *J. Am. Chem. Soc.* **2013**, *135*, 14520–14523.

(24) Chirmanov, V.; Stanish, P. C.; Layek, A.; Radovanovic, P. V. Distance-Dependent Energy Transfer between Ga2O3 Nanocrystal Defect States and Conjugated Organic Fluorophores in Hybrid White-Light-Emitting Nanophosphors. *J. Phys. Chem. C* **2015**, *119*, 5687–5696.

(25) Das, S.; Manam, J.; Sharma, S. K. Composites of BaAl2O4:Eu2+,Dy3+/organic dye encapsulated in mesoporous silica as multicolor long persistent phosphors based on radiative energy transfer. *New J. Chem.* **2017**, *41*, 5934–5941.

(26) Langdon-Jones, E. E.; Lloyd, D.; Hayes, A. J.; Wainwright, S. D.; Mottram, H. J.; Coles, S. J.; Horton, P. N.; Pope, S. J. A. Alkynyl-naphthalimide Fluorophores: Gold Coordination Chemistry and Cellular Imaging Applications. *Inorg. Chem.* **2015**, *54*, 6606–6615.

(27) Schachtschneider, A.; Wessig, M.; Spitzbarth, M.; Donner, A.; Fischer, C.; Drescher, M.; Polarz, S. Directional MaterialsNanoporous Organosilica Monoliths with Multiple Gradients Prepared Using Click Chemistry. *Angew. Chem., Int. Ed.* **2015**, *54*, 10465–10469.

(28) Savell, K. E.; Gallus, N. V. N.; Simon, R. C.; Brown, J. A.; Revanna, J. S.; Osborn, M. K.; Song, E. Y.; O’Malley, J. J.; Stackhouse, C. T.; Norvil, A.; Gowher, H.; Sweatt, J. D.; Day, J. J. Extra-coding RNAs regulate neuronal DNA methylation dynamics. *Nat. Commun.* **2016**, *7*, 12091.

(29) Yang, J. X.; Wang, X. L.; Tusong; Xu, L. H. Studies on the synthesis and spectral properties of novel 4-benzofuranyl-1,8-naphthalimide derivatives. *Dyes Pigm.* **2005**, *67*, 27–33.

(30) Jiang, W.; Tang, J. N.; Qi, Q.; Wu, W. B.; Sun, Y. M.; Fu, D. W. The synthesis, crystal structure and photophysical properties of three novel naphthalimide dyes. *Dyes Pigm.* **2009**, *80*, 11–16.

(31) Ren, J.; Zhao, X. L.; Wang, Q. C.; Ku, C. F.; Qu, D. H.; Chang, C. P.; Tian, H. Synthesis and fluorescence properties of novel co-facial folded naphthalimide dimers. *Dyes Pigm.* **2005**, *64*, 179–186.

(32) Chen, G. D.; Wang, L. Z.; Zhang, J. L.; Chen, F.; Anpo, M. Photophysical properties of a naphthalimide derivative encapsulated within Si-MCM-41, Ce-MCM-41 and Al-MCM-41. *Dyes Pigm.* **2009**, *81*, 119–123.

(33) Chin, S. L. Further evidence of dimer emission from super radiant travellin-wave laser of concentrated aqueous-solution of rhodamine 6G and rhodamine B. *Phys. Lett. A* **1974**, *A48*, 403–404.

(34) Deutsch, T. F.; Bass, M.; Meyer, P.; Protopap, S. EMISSION SPECTRUM OF RHODAMINE B DYE LASERS. *Appl. Phys. Lett.* **1967**, *11*, 379.

(35) Rao, H. H.; Xue, Z. H.; Zhao, G. H.; Li, S. Y.; Du, X. Z. Fluorescence emission properties of rhodamine B encapsulated organic-inorganic hybrid mesoporous silica host. *J. Non-Cryst. Solids* **2016**, *450*, 32–37.

(36) Badley, R. D.; Ford, W. T.; McEnroe, F. J.; Assink, R. A. Surface modification of colloidal silica. *Langmuir* **1990**, *6*, 792–801.

(37) Philipse, A. P.; Vrij, A. Preparation and properties of nonaqueous model dispersions of chemically modified, charged silica spheres. *J. Colloid Interface Sci.* **1989**, *128*, 121–136.

(38) Achatz, D. E.; Heilitag, F. J.; Li, X. H.; Link, M.; Wolfbeis, O. S. Colloidal silica nanoparticles for use in click chemistry-based conjugations and fluorescent affinity assays. *Sens. Actuators, B* **2010**, *150*, 211–219.

(39) David, S. L.; Michail, C. M.; Valais, I. G.; Toutountzis, A. E.; Liaparinos, P. F.; Cavouras, D. A.; Kandarakis, I. S.; Panayiotakis, G.

S. Investigation of Luminescence Properties of Lu₂SiO₅:Ce (LSO) Powder Scintillator in the X-Ray Radiography Energy Range. *IEEE Trans. Nucl. Sci.* **2008**, *55*, 3684–3691.

(40) Suzuki, H.; Tombrello, T. A.; Melcher, C. L.; Schweitzer, J. S. Light emission mechanism of Lu₂(SiO₄)O-Ce. *IEEE Trans. Nucl. Sci.* **1993**, *40*, 380–383.

(41) Ren, G. H.; Qin, L. S.; Lu, S.; Li, H. Y. Scintillation characteristics of lutetium oxyortho silicate (Lu₂SiO₅: Ce) crystals doped with cerium ions. *Nucl. Instrum. Methods Phys. Res., Sect. A* **2004**, *531*, 560–565.

(42) Kirm, M.; Lushchik, A.; Lushchik, C.; Zimmerer, G. Investigation of luminescence properties of pure and Ce³⁺ doped Y₃Al₅O₁₂ crystals using VUV radiation. *ECS Proceedings* **2000**, *99*, 113–122.

(43) Xu, C.; Qu, X. G. Cerium oxide nanoparticle: a remarkably versatile rare earth nanomaterial for biological applications. *NPG Asia Mater.* **2014**, *6*, e90.

(44) Moutet, P.; Sangeetha, N. M.; Ressier, L.; Vilar-Vidal, N.; Comesana-Hermo, M.; Ravaine, S.; Vallee, R. A. L.; Gabudean, A. M.; Astilean, S.; Farcau, C. Surface-enhanced spectroscopy on plasmonic oligomers assembled by AFM nanoxerography. *Nanoscale* **2015**, *7*, 2009–2022.

(45) Piok, T.; Gadermaier, C.; Wenzl, F. P.; Patil, S.; Montenegro, R.; Landfester, K.; Lanzani, G.; Cerullo, G.; Scherf, U.; List, E. J. W. The photophysics of organic semiconducting nanospheres: a comprehensive study. *Chem. Phys. Lett.* **2004**, *389*, 7–13.

(46) Pignalosa, P.; Liu, B.; Chen, H.; Smith, H.; Yi, Y. S. Giant light extraction enhancement of medical imaging scintillation materials using biologically inspired integrated nanostructures. *Opt. Lett.* **2012**, *37*, 2808–2810.

(47) Al-Juboori, S. I.; Dondzillo, A.; Stubblefield, E. A.; Felsen, G.; Lei, T. C.; Klug, A. Light Scattering Properties Vary across Different Regions of the Adult Mouse Brain. *PLoS One* **2013**, *8*, e67626.

(48) Long, M. A.; Fee, M. S. Using temperature to analyse temporal dynamics in the songbird motor pathway. *Nature* **2008**, *456*, 189–194.

(49) Harry, G. J.; Billingsley, M.; Bruinink, A.; Campbell, I. L.; Classen, W.; Dorman, D. C.; Galli, C.; Ray, D.; Smith, R. A.; Tilson, H. A. In vitro techniques for the assessment of neurotoxicity. *Environ. Health Perspect.* **1998**, *106*, 131–158.

(50) Berry, R.; Getzin, M.; Gjesteby, L.; Wang, G. X-Optogenetics and U-Optogenetics: Feasibility and Possibilities. *Photonics* **2015**, *2*, 23–39.

(51) Boyden, E. S.; Zhang, F.; Bamberg, E.; Nagel, G.; Deisseroth, K. Millisecond-timescale, genetically targeted optical control of neural activity. *Nat. Neurosci.* **2005**, *8*, 1263–1268.